Level-resolved R-matrix calculations for the electron-impact excitation of Ne^{3+} and Ne^{6+}

J. A. Ludlow, T. G. Lee, C. P. Ballance, S. D. Loch, and M. S. Pindzola
Department of Physics, Auburn University, Auburn, Alabama 36849, USA
(Received 22 June 2011; published 1 August 2011)

Large-scale R-matrix calculations are carried out for the electron-impact excitation of Ne^{3+} and Ne^{6+}. For Ne^{3+}, a 581-LSJ-level R-matrix intermediate coupling frame transformation calculation is made for excitations up to the $n = 4$ shell. For some transitions, large effective collision strength differences are found with current 23-jKJ-level Breit-Pauli R-matrix and earlier 22-LSJ-level R-matrix jj omega (JAJOM) calculations. For Ne^{6+}, a 171-jKJ-level Breit-Pauli R-matrix calculation is made for excitations up to the $n = 5$ shell. For some transitions, large effective collision strength differences are found with current 46-jKJ-level Breit-Pauli R-matrix and earlier 46-LSJ-level R-matrix JAJOM calculations. Together with existing R-matrix calculations for other ion stages, high-quality excitation data are now available for astrophysical and laboratory plasma modeling along the entire Ne isonuclear sequence.

DOI: 10.1103/PhysRevA.84.022701 PACS number(s): 34.80.Dp

I. INTRODUCTION

Electron-impact excitation of Ne ions is an important process in the modeling of astronomical and laboratory plasmas. For example, in controlled magnetic fusion, gaseous Ne is often pufffed into the tokamak edge in order to cool the plasma [1]. In astrophysics, the presence of Ne ions in planetary nebulae serves as important temperature and density diagnostics [2]. The generation of benchmark electron-impact excitation data for the Ne isonuclear sequence is therefore of significant interest.

The R-matrix method was first applied to calculate nonrelativistic LS term-resolved cross sections for the electron-impact excitation of light atoms and their ions [3]. Transformation of the physical S matrices in LS coupling using the jj omega (JAJOM) method [4] allows the calculation of level-resolved cross sections, while transformation of the unphysical S matrices in LS coupling using the intermediate-coupling frame transformation (ICFT) method [5] also allows the calculation of level-resolved cross sections. The R matrix was extended to directly calculate semirelativistic (Breit-Pauli) jKJ level-resolved cross sections [6] and fully relativistic (Dirac) jjJ level-resolved cross sections [7] for the electron-impact excitation of heavy atoms and their ions. All of the standard R-matrix methods have also been extended to include the coupling of the bound states to the target continuum using the R matrix with pseudostates (RMPS) method [8,9].

Benchmark electron-impact excitation data already exist for quite a few of the atomic ions in the Ne isonuclear sequence. For neutral Ne, a 235-jKJ-level Breit-Pauli RMPS calculation has been performed [10]. For Ne^+, a 138-LSJ-level R-matrix ICFT calculation [11] included excitations up to the $n = 4$ shell. For Ne^{2+}, a recent large-scale 554-LSJ-level R-matrix ICFT calculation [12] included excitations up to the $n = 4$ shell, building on earlier 56-LSJ-level R-matrix JAJOM and 56-jKJ-level Breit-Pauli R-matrix calculations [13,14]. For Ne^{4+}, a 138-LSJ-level R-matrix ICFT calculation [15] included excitations up to the $n = 3$ subshell. For Ne^{5+}, a 180-LSJ-level R-matrix ICFT calculation [16] included excitations up to the $n = 4$ subshell.

The highly charged members of the sequence, namely, Ne^{7+}, Ne^{8+}, and Ne^{9+}, have been the subject of a number of recent studies. For Ne^{7+}, there has been a recent 24-jjJ-level Dirac R-matrix calculation [17] that included excitations up to the $n = 5$ shell. For Ne^{8+}, there has been a 49-jjJ-level Dirac R-matrix calculation [18] that included excitations up to the $n = 5$ shell. For Ne^{9+}, there has been a recent 25-jjJ-level Dirac R-matrix calculation [19] that included excitations up to the $n = 5$ shell.

In this paper we shall focus on the electron-impact excitation of Ne^{3+} and Ne^{6+}, since the reliable data available is limited and the theoretical work that exists for these ions to date has been confined to older, small-scale and less sophisticated calculations. For Ne^{3+}, the earliest calculations were performed by Saraph *et al.* [20]. They utilized a distorted-wave method to evaluate collision strengths for transitions between the $1s^2 2s^2 2p^3$ ^4S, ^2D, and ^2P terms. The same method was also used in their following paper [21] to evaluate collision strengths for transitions among the $^4S_{3/2}$, $^2D_{3/2,5/2}$, and $^2P_{1/2,3/2}$ levels. Both calculations were quite limited in that resonance effects were excluded. Later, close-coupling calculations [22,23], including the ground and first excited configurations, gave rise to near-threshold resonances in the cross sections for all ten fine-structure transitions within the ground configuration of Ne^{3+}. The most recent work to date for electron-impact excitation of Ne^{3+} is a 22-LSJ-level R-matrix JAJOM calculation [24,25] including excitations up to the $3s$ subshell. For Ne^{6+}, there are early 6-LS-term R-matrix calculations [26,27]. More recently, 46-LSJ-level R-matrix JAJOM calculations [28,29] have been made including excitations to the $n = 3$ shell. Therefore, in this paper we carry out a 581-LSJ-level R-matrix ICFT calculation for Ne^{3+} and a 171-jKJ-level Breit-Pauli R-matrix calculation for Ne^{6+} to complete the high-quality excitation data now available for astrophysical and laboratory plasma modeling along the entire Ne isonuclear sequence.

The rest of the paper is structured as follows: details of the atomic structure and scattering methods are given in Sec. II, electron-impact excitation cross sections for Ne^{3+} are presented in Sec. III A, electron-impact excitation cross sections for Ne^{6+} are presented in Sec. III B, radiated power loss functions for Ne^{6+} are presented in Sec. III C, and a brief summary is given in Sec. IV. Unless otherwise stated, we will use atomic units throughout.

II. ATOMIC STRUCTURE AND SCATTERING METHODS

To determine the radial orbitals for the spectroscopic states, the atomic structure code AUTOSTRUCTURE [30] was used with the aid of the Graphical AutoStructure Package (GASP) [31], a java front end to AUTOSTRUCTURE. The radial orbitals were calculated using a Thomas-Fermi-Dirac-Amaldi statistical potential using Breit-Pauli intermediate coupling. For Ne^{3+}, the $1s$–$4f$ subshells were included in the configurations $1s^22s^22p^3$, $1s^22s^22p^2nl$ $(n = 3$–$4, l = 0$–$3)$, $1s^22s2p^4$, $1s^22s2p^3nl$ $(n = 3$–$4, l = 0$–$3)$, $1s^22p^5$, and $1s^22p^43l$ $(l = 0$–$2)$, giving rise to 581 levels. In order to obtain accurate energies, it was necessary to adjust the radial extent of the orbitals via a scaling parameter λ_{nl}. The scaling parameters were tuned to $\lambda_{1s} = 1.36$, $\lambda_{2s} = 1.52$, $\lambda_{2p} = 1.03$, $\lambda_{3s} = 1.45$, $\lambda_{3p} = 1.25$, $\lambda_{3d} = 1.40$, $\lambda_{4s} = 1.05$, $\lambda_{4p} = 1.03$, $\lambda_{4d} = 1.05$, and $\lambda_{4f} = 1.20$. The scaling parameter choices give good agreement between the theoretical and experimental [32] energies for Ne^{3+}. For Ne^{6+}, the $1s$–$5g$ subshells were included in the configurations $1s^22s^2$, $1s^22s2p$, $1s^22snl$ $(n = 3$–$5, l = 0$–$5)$, $1s^22p^2$, $1s^22pnl$ $(n = 3$–$5, l = 0$–$5)$, and $1s2s^22p$, giving rise to 171 levels. The radial scaling parameters λ_{nl} were all set to 1.00. The scaling parameter choices give good agreement between the theoretical and experimental [32] energies for Ne^{6+}.

The scattering calculations are performed using the R-matrix method making use of a suite of parallel R-matrix codes [33,34]. A 581-LSJ-level R-matrix ICFT calculation was performed for the electron-impact excitation of Ne^{3+}. The R-matrix box size was 17.35 a.u. and 40 $(N + 1)$-electron continuum basis orbitals per angular momentum were used. A 171-jKJ-level Breit-Pauli R-matrix calculation was performed for the electron-impact excitation of Ne^{6+}. The R-matrix box size was 14.57 a.u. and 50 $(N + 1)$-electron continuum basis orbitals per angular momentum were used. The outer region calculations for Ne^{3+} and Ne^{6+} made use of a fine energy mesh consisting of 40,000 energy points below the ionization threshold in order to properly resolve resonance structure and to achieve converged effective collision strengths in the chosen temperature range. The collision strength for an $i \rightarrow j$ transition is given by

$$\Omega_{ij} = \frac{w_i \epsilon_i}{2\pi} \sigma_{ij}, \tag{1}$$

where w_i is the statistical weight of the initial level, ϵ_i is the incident energy, and σ_{ij} is the cross section for an $i \rightarrow j$ transition. The effective collision strength for an $i \rightarrow j$ transition is given by

$$\langle \Omega_{ij} \rangle_{\text{eff}} = \int_0^\infty \Omega_{ij} e^{-\epsilon_j / kT_e} d(\epsilon_j / kT_e), \tag{2}$$

where ϵ_j is the final energy and T_e is the electron temperature.

III. RESULTS

A. Electron-impact excitation of Ne^{3+}

Collision strengths for selected transitions from the 581-LSJ-level R-matrix ICFT calculation are presented in Fig. 1. To facilitate comparisons with the older 22-LSJ-level R-matrix JAJOM calculation [24,25], a 23-jKJ-level Breit-Pauli R-matrix calculation was performed using the same configurations used in the older R-matrix calculation, namely, $1s^22s^22p^3$, $1s^22s2p^4$, $1s^22p^5$, and $1s^22s^22p^23s$. Our 23-jKJ-level calculation includes the $1s^22s^22p^23s\ ^2S_{1/2}$ level, which is not included in the earlier 22-LSJ-level calculation. Collision strengths for the same selected transitions from the 23-jKJ-level Breit-Pauli R-matrix calculation are also presented in Fig. 1. Effective collision strengths for the selected transitions from the 581-LSJ-level R-matrix ICFT, 23-jKJ-level Breit-Pauli R-matrix, and 22-LSJ-level R-matrix JAJOM calculations are presented in Fig. 2.

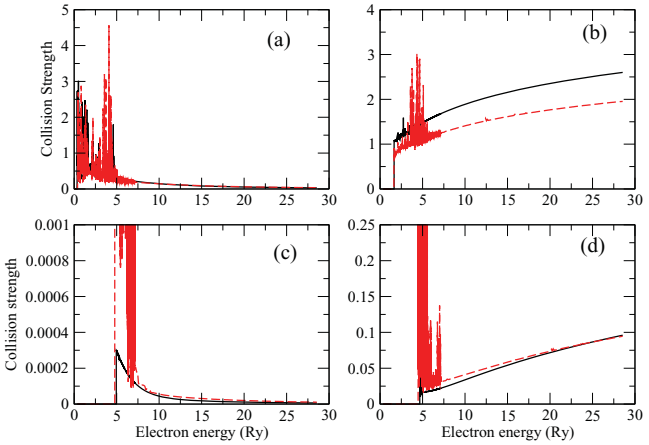

FIG. 1. (Color online) Collision strengths for electron impact excitation of Ne^{3+}: (a) $1s^22s^22p^3\ ^4S_{3/2} \rightarrow 1s^22s^22p^3\ ^2D_{3/2}$, (b) $1s^22s^22p^3\ ^4S_{3/2} \rightarrow 1s^22s2p^4\ ^4P_{1/2}$, (c) $1s^22s^22p^3\ ^4S_{3/2} \rightarrow 1s^22s^22p^23s\ ^2D_{3/2}$, and (d) $1s^22s^22p^3\ ^4S_{3/2} \rightarrow 1s^22s^22p^23s\ ^4P_{1/2}$. The black solid line is the 23-jKJ-level Breit-Pauli R-matrix calculation, and the red dashed line is the 581-LSJ-level R-matrix ICFT calculation.

For the transition between the $1s^22s^22p^3\ ^4S_{3/2}$ and $1s^22s^22p^3\ ^2D_{3/2}$ levels, found in Fig. 1(a), there is good

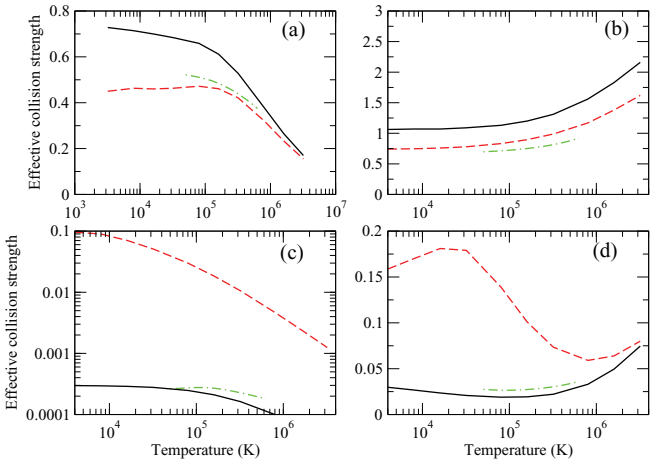

FIG. 2. (Color online) Effective collision strengths for electron-impact excitation of Ne^{3+}: (a) $1s^22s^22p^3\ ^4S_{3/2} \rightarrow 1s^22s^22p^3\ ^2D_{3/2}$, (b) $1s^22s^22p^3\ ^4S_{3/2} \rightarrow 1s^22s2p^4\ ^4P_{1/2}$, (c) $1s^22s^22p^3\ ^4S_{3/2} \rightarrow 1s^22s^22p^23s\ ^2D_{3/2}$, and (d) $1s^22s^22p^3\ ^4S_{3/2} \rightarrow 1s^22s^22p^23s\ ^4P_{1/2}$. The black solid line is the 23-jKJ-level Breit-Pauli R-matrix calculation, the red dashed line is the 581-LSJ-level R-matrix ICFT calculation, and the green dot-dashed line is the 22-LSJ-level R-matrix JAJOM calculation [25].

agreement in the background collision strengths for the 581-LSJ-level R-matrix ICFT and the 23-jKJ-level Breit-Pauli R-matrix calculations. However, the two calculations show very different resonance contributions. This is reflected in a 50% difference in the effective collision strengths of the large and small calculations, as seen in Fig. 2(a). The transitions between the $1s^2 2s^2 2p^3\ ^4S_{3/2}$ and $1s^2 2s 2p^4\ ^2P_{1/2}$ levels, found in Fig. 1(b), show differences both in the background and in the resonance contributions to the collision strengths. The smaller background collision strength for the 581-LSJ-level R-matrix ICFT calculation leads to a smaller effective collision strength, as seen in Fig. 2(b).

For transitions between the $n = 2$ and $n = 3$ shells, there are even larger differences between the collision strengths found in Figs. 1(c) and 1(d) for the 581-LSJ-level R-matrix ICFT and 23-jKJ-level Breit-Pauli R-matrix calculations. There are also large differences between the effective collision strengths found in Figs. 2(c) and 2(d) for the 581-LSJ-level R-matrix ICFT calculations and 23-jKJ-level Breit-Pauli R-matrix calculations. While these differences are largely due to the extra resonant contributions present in the larger calculations, there are also differences in the background collision strengths. In comparison, the smaller calculations have negligible resonance contributions above the $3s$ threshold. We note that differences between the effective collision strengths found in Figs. 2(a) and 2(b) for the 23-jkJ-level Breit-Pauli R-matrix and 22-LSJ-level R-matrix JAJOM calculations are due to the $3\bar{p}$, $3\bar{d}$, and $4\bar{s}$ pseudostates included in the more accurate 22-LSJ-level R-matrix JAJOM atomic structure calculations. Atomic structure effects are not as important in the transitions between the $n = 2$ and $n = 3$ shells, so there is reasonable agreement between the effective collision strengths found in Figs. 2(c) and 2(d) for the 23-jKJ-level Breit-Pauli R-matrix and 22-LSJ-level R-matrix JAJOM calculations.

B. Electron-impact excitation of Ne^{6+}

Collision strengths for selected transitions from the 171-jKJ-level Breit-Pauli R-matrix calculation are presented in Fig. 3. To facilitate comparisons with the older 46-LSJ-level R-matrix JAJOM calculation [28,29], a 46-jKJ-level Breit-Pauli R-matrix calculation was performed using the same configurations used in the older R-matrix calculation, namely, $1s^2 2s^2$, $1s^2 2s 2p$, $1s^2 2s 3l$ ($l = 0$–2), $1s^2 2p^2$, and $1s^2 2p 3l$ ($l = 0$–2). Collision strengths for the same selected transitions from the 46-jKJ-level Breit-Pauli R-matrix calculation are also presented in Fig. 3. Effective collision strengths for the selected transitions from the 171-jKJ-level Breit-Pauli R-matrix, 46-jKJ-level Breit-Pauli R-matrix, and 46-LSJ-level R-matrix JAJOM calculations are presented in Fig. 4.

For transitions within the $n = 2$ shell, there is reasonable agreement between the background collision strengths, found in Figs. 3(a) and 3(b), for the 171-jKJ-level Breit-Pauli R-matrix and the 46-jKJ-level Breit-Pauli R-matrix calculations. The larger calculation has extra resonance contributions attached to the $n = 4$ and $n = 5$ thresholds. This leads to large differences in the effective collision strengths above 3.0×10^5 K, as seen in Figs. 4(a) and 4(b).

For transitions between the $n = 2$ and $n = 3$ shells, there are even larger differences between the collision strengths,

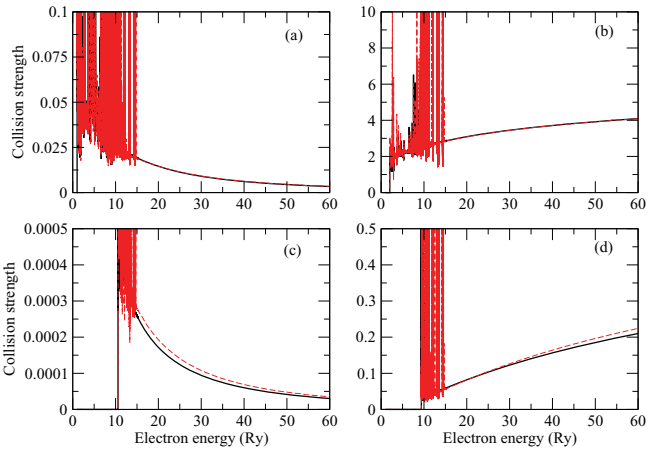

FIG. 3. (Color online) Collision strengths for electron-impact excitation of Ne^{6+}: (a) $1s^2 2s^2\ ^1S_0 \rightarrow 1s^2 2s 2p\ ^3P_1$, (b) $1s^2 2s^2\ ^1S_0 \rightarrow 1s^2 2s 2p\ ^1P_1$, (c) $1s^2 2s^2\ ^1S_0 \rightarrow 1s^2 2p 3p\ ^3D_1$, and (d) $1s^2 2s^2\ ^1S_0 \rightarrow 1s^2 2s 3p\ ^1P_1$. The black solid line is the 46-jKJ-level Breit-Pauli R-matrix calculation and the red dashed line is the 171-jKJ-level Breit-Pauli R-matrix calculation.

found in Figs. 3(c) and 3(d), for the 171-jKJ-level Breit-Pauli R-matrix and 46-jKJ-level Breit-Pauli R-matrix calculations at all energies. There are also large differences between the effective collision strengths, found in Figs. 4(c) and 4(d), for the 171-jKJ-level Breit-Pauli R-matrix and 46-jKJ-level Breit-Pauli R-matrix calculations at all electron temperatures. The differences are again largely due to resonant contributions not present in the smaller calculations. We note that there is reasonable agreement between the effective collision strengths found in Figs. 4(a)–4(d) for the 46-jKJ-level Breit-Pauli R-matrix and 46-LSJ-level R-matrix JAJOM calculations.

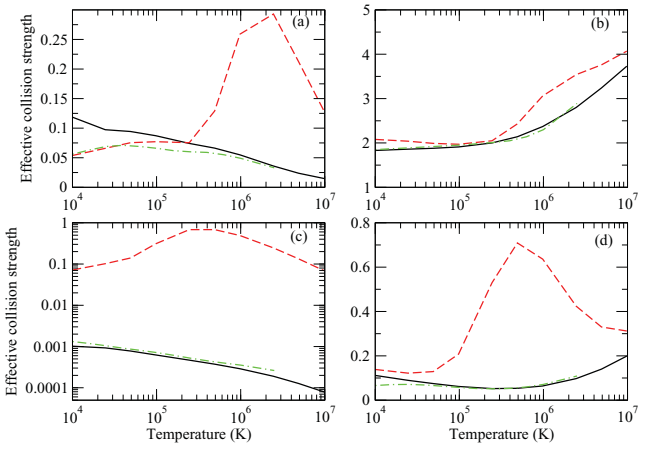

FIG. 4. (Color online) Effective collision strengths for electron-impact excitation of Ne^{6+}: (a) $1s^2 2s^2\ ^1S_0 \rightarrow 1s^2 2s 2p\ ^3P_1$, (b) $1s^2 2s^2\ ^1S_0 \rightarrow 1s^2 2s 2p\ ^1P_1$, (c) $1s^2 2s^2\ ^1S_0 \rightarrow 1s^2 2p 3p\ ^3D_1$, and (d) $1s^2 2s^2\ ^1S_0 \rightarrow 1s^2 2s 3p\ ^1P_1$. The black solid line is the 46-jKJ-level Breit-Pauli R-matrix calculation, the red dashed line is the 171-jKJ-level Breit-Pauli R-matrix calculation, and the green dot-dashed line is the 46-LSJ-level R-matrix JAJOM calculation [29].

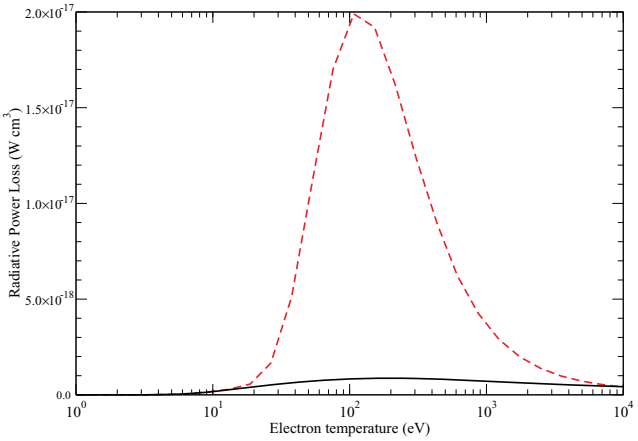

FIG. 5. (Color online) Radiated power loss functions for Ne^{6+}. The black solid line is from the 46-jKJ-level Breit-Pauli R-matrix calculation and the red dashed line is from the 171-jKJ-level Breit-Pauli R-matrix calculation.

C. Radiated power loss for Ne^{6+}

As an example of the benefits of improved electron-impact excitation cross sections, we calculate the radiated power loss for Ne^{6+} involving the 46 levels found in the $1s^22s^2$, $1s^22s2p$, $1s^22s3l$ ($l = 0$–2), $1s^22p^2$, and $1s^22p3l$ ($l = 0$–2) configurations. Solving the generalized collisional radiative equations [35], we first determine the population abundance N_j for each excited level of Ne^{6+}. The radiated power loss function is given by [35]

$$R_{\rm PL}(T_e,N_e) = \sum_{jk} A_{j\to k}\Delta E_{jk}\frac{N_j}{N_eN_1}, \qquad (3)$$

where $A_{j\to k}$ is the spontaneous emission rate, ΔE_{jk} is the corresponding transition energy, T_e is the electron temperature, N_e is the electron density, and N_1 is the Ne^{6+} ion density in the ground level. The radiated power loss functions for Ne^{6+} at $N_e = 1.0\times10^6$ cm^{-3}, involving the same 46 levels in both the 171-jKJ-level Breit-Pauli R-matrix and 46-jKJ-level Breit-Pauli R-matrix calculations, are presented in Fig. 5. Due to much stronger resonance enhancements of the excitation cross sections, the radiated power loss function for the 171-jKJ-level Breit-Pauli R-matrix calculation is an order of magnitude larger than the radiated power loss function for the 46-jKJ-level Breit-Pauli R-matrix calculation at an electron temperature of 100 eV. We note that the total fractional abundance for Ne^{6+} peaks around 100 eV.

IV. SUMMARY

As part of a project to generate benchmark electron-impact excitation data for the Ne isonuclear sequence, atomic data has been calculated for Ne^{3+} and Ne^{6+}. The importance of the inclusion of higher n shells was demonstrated for transitions between the $n = 2$ and $n = 3$ shells for both Ne^{3+} and Ne^{6+}. The effect of this atomic data on radiative power loss for Ne^{6+} was also presented. Our final effective collision strengths will be made available in the Atomic Data and Analysis Structure (ADAS) database [36]. In future work, the major challenge remaining in the Ne isonuclear sequence will be to extend the initial 235-jKJ-level Breit-Pauli RMPS calculation for neutral Ne [10] to energies above the ionization limit.

ACKNOWLEDGMENTS

We wish to thank Dr. Martin O'Mullane for helpful discussions. This work was supported in part by grants from the US Department of Energy. Computational work was carried out at the National Energy Research Scientific Computing Center in Oakland, California and at the National Institute for Computational Sciences in Knoxville, Tennessee.

[1] H. D. Pacher, A. S. Kukushkin, G. W. Pacher, V. Kotov, G. Janeschitz, D. Reiter, and D. P. Coster, J. Nucl. Mater. **390-391**, 259 (2009).
[2] J. E. Herald, L. Bianchi, and D. J. Hillier, Astrophys. J. **627**, 424 (2005).
[3] P. G. Burke and W. D. Robb, Adv. At., Mol., Phys. **11**, 143 (1975).
[4] H. E. Saraph, Comput. Phys. Commun. **15**, 247 (1978).
[5] D. C. Griffin, N. R. Badnell, and M. S. Pindzola, J. Phys. B **31**, 3713 (1998).
[6] K. A. Berrington, W. B. Eissner, and P. H. Norrington, Comput. Phys. Commun. **92**, 290 (1995).
[7] P. H. Norrington and I. P. Grant, J. Phys. B **20**, 4869 (1987).
[8] K. Bartschat, E. T. Hudson, M. P. Scott, P. G. Burke, and V. M. Burke, J. Phys. B **29**, 115 (1996).
[9] T. W. Gorczyca and N. R. Badnell, J. Phys. B **30**, 3897 (1997).
[10] C. P. Ballance and D. C. Griffin, J. Phys. B **37**, 2943 (2004).
[11] D. C. Griffin, D. M. Mitnik, and N. R. Badnell, J. Phys. B **34**, 4401 (2001).
[12] B. M. McLaughlin, T.-G. Lee, J. A. Ludlow, E. Landi, S. D. Loch, C. P. Ballance, and M. S. Pindzola, J. Phys. B (to be published).
[13] B. M. McLaughlin and K. L. Bell, J. Phys. B **33**, 597 (2000).
[14] B. M. McLaughlin, A. Daw, and K. L. Bell, J. Phys. B **35**, 283 (2002).
[15] D. C. Griffin and N. R. Badnell, J. Phys. B **33**, 4389 (2000).
[16] D. M. Mitnik, D. C. Griffin, and N. R. Badnell, J. Phys. B **34**, 4455 (2001).
[17] K. M. Aggarwal, F. P. Keenan, and R. F. Heeter, Phys. Scr. **81**, 015303 (2010).
[18] G. X. Chen, R. K. Smith, K. Kirby, N. S. Brickhouse, and B. J. Wargelin, Phys. Rev. A **74**, 042709 (2006).
[19] K. M. Aggarwal, F. P. Keenan, and R. F. Heeter, Phys. Scr. **82**, 015006 (2010).
[20] H. E. Saraph, M. J. Seaton, and J. Shemming, Philos. Trans. R. Soc. London **77**, 264 (1969).
[21] P. de A. P. Martin, H. E. Saraph, and M. J. Seaton, J. Phys. B **2**, 427 (1969).

[22] K. Giles, Mon. Not. R. Astron. Soc. **195**, 63 (1981).
[23] A. K. Giles and S. O. Kastner, Astrophys. J. **332**, 1063 (1988).
[24] C. A. Ramsbottom, K. L. Bell, and F. P. Keenan, Mon. Not. R. Astron. Soc. **293**, 233 (1998).
[25] C. A. Ramsbottom and K. L. Bell, At. Data Nucl. Data Tables **68**, 203 (1998).
[26] P. L. Dufton, J. G. Doyle, and A. E. Kingston, Astron. Astrophys. **78**, 318 (1979).
[27] C. Mendoza, in *Planetary Nebulae*, edited by D. R. Flower (Reidel, Dordrecht, 2003), Vol. 103, p. 143.
[28] C. A. Ramsbottom, K. A. Berrington, and K. L. Bell, J. Phys. B **27**, L811 (1994).
[29] C. A. Ramsbottom, K. A. Berrington, and K. L. Bell, At. Data Nucl. Data Tables **61**, 105 (1995).
[30] N. R. Badnell, J. Phys. B **30**, 1 (1997).
[31] See [http://vanadium.rollins.edu/GASP.html].
[32] See [http://physics.nist.gov/PhysRefData].
[33] D. M. Mitnik, M. S. Pindzola, D. C. Griffin, and N. R. Badnell, J. Phys. B **32**, L479 (1999).
[34] C. P. Ballance and D. C. Griffin, J. Phys. B **37**, 2943 (2004).
[35] S. D. Loch, C. J. Fontes, J. Colgan, M. S. Pindzola, C. P. Ballance, D. C. Griffin, M. G. O'Mullane, and H. P. Summers, Phys. Rev. E **69**, 066405 (2004).
[36] See [http://www.adas-data.ac.uk].